Silencing of ceramide synthase 2 in hepatocytes modulates plasma ceramide biomarkers predictive of cardiovascular death

Schmidt, Steffen; Gallego, Sandra F; Zelnik, Iris Daphne; Kovalchuk, Sergey; Albæk, Nanna; Sprenger, Richard R; Øverup, Charlotte; Pewzner-Jung, Yael; Futerman, Anthony H; Lindholm, Marie W; Jensen, Ole N; Ejsing, Christer S

Published in:
Molecular Therapy

DOI:
10.1016/j.ymthe.2021.08.021

Publication date:
2022

Document version:
Final published version

Molecular Therapy
Original Article

Silencing of ceramide synthase 2 in hepatocytes modulates plasma ceramide biomarkers predictive of cardiovascular death

Steffen Schmidt,[1] Sandra F. Gallego,[2] Iris Daphne Zelnik,[3] Sergey Kovalchuk,[2] Nanna Albæk,[1] Richard R. Sprenger,[2] Charlotte Øverup,[1] Yael Pewzner-Jung,[3] Anthony H. Futerman,[3] Marie W. Lindholm,[1] Ole N. Jensen,[2] and Christer S. Ejsing[2,4]

[1]Roche Pharma Research and Early Development, Roche Innovation Center Copenhagen, 2970 Hørsholm, Denmark; [2]Department of Biochemistry and Molecular Biology, VILLUM Center for Bioanalytical Sciences, University of Southern Denmark, 5230 Odense, Denmark; [3]Department of Biomolecular Sciences, Weizmann Institute of Science, Rehovot 7610001, Israel; [4]Cell Biology and Biophysics Unit, European Molecular Biology Laboratory, 69117 Heidelberg, Germany

Emerging clinical data show that three ceramide molecules, Cer d18:1/16:0, Cer d18:1/24:1, and Cer d18:1/24:0, are biomarkers of a fatal outcome in patients with cardiovascular disease. This finding raises basic questions about their metabolic origin, their contribution to disease pathogenesis, and the utility of targeting the underlying enzymatic machinery for treatment of cardiometabolic disorders. Here, we outline the development of a potent *N*-acetylgalactosamine-conjugated antisense oligonucleotide engineered to silence ceramide synthase 2 specifically in hepatocytes *in vivo*. We demonstrate that this compound reduces the ceramide synthase 2 mRNA level and that this translates into efficient lowering of protein expression and activity as well as Cer d18:1/24:1 and Cer d18:1/24:0 levels in liver. Intriguingly, we discover that the hepatocyte-specific antisense oligonucleotide also triggers a parallel modulation of blood plasma ceramides, revealing that the biomarkers predictive of cardiovascular death are governed by ceramide biosynthesis in hepatocytes. Our work showcases a generic therapeutic framework for targeting components of the ceramide enzymatic machinery to disentangle their roles in disease causality and to explore their utility for treatment of cardiometabolic disorders.

INTRODUCTION

Ceramides are bioactive lipids with crucial roles in biochemical processes that impinge on the pathophysiology of metabolic and cardiovascular diseases, including energy metabolism, apoptosis, and inflammation.[1–3] Emerging clinical data have recently revealed a strong association between unique ceramide molecules in the circulation and the mortality of patients with cardiovascular disease (CVD)[4–6] as well as the development of type 2 diabetes.[7–9] Specifically, Cer d18:1/16:0 and Cer d18:1/24:1 are reported to be high-risk markers for a fatal outcome of patients with coronary artery disease whereas Cer d18:1/24:0 is a protective marker.[4] These findings have prompted routine testing of ceramides in clinical settings to provide independent and added value to traditional markers of cardiometabolic conditions, such as low-density lipoprotein (LDL) cholesterol.[6,10] Despite this great progress and its improved stratification of patients in preventive healthcare, many questions concerning the metabolic origin of the ceramide biomarkers, their mechanistic contribution to disease pathogenesis, as well as the therapeutic utility of targeting the underlying enzymatic machinery for treatment of cardiometabolic disorders remain unexplored.

Ceramides are a diverse class of sphingolipids, composed of a long-chain base and an amide-linked fatty acyl chain with variable lengths, typically ranging from 14 to 24 carbon atoms and having 0 or 1 double bond.[11,12] Their biosynthesis is an essential module within the more extensive sphingolipid metabolic network, which commences with the condensation of serine and activated palmitoyl (16:0)-coenzyme A (CoA) and ends with the production and turnover of more complex sphingolipids, including sphingomyelins (SMs) and glycosphingolipids (Figure 1A). Six ceramide synthases (CerSs) exist in mammals and are the prime determinants of ceramide molecular heterogeneity. These enzymes vary in tissue distribution and substrate specificity.[12–15] Especially, CerS1, CerS2, CerS5, and CerS6 have been shown to be of relevance for cardiometabolic disorders. CerS1 is responsible for the synthesis of ceramides with primarily C_{18}-fatty acyl chains in neural tissue and skeletal muscle, which for the latter has been reported to positively influence glucose homeostasis,[16] thereby supporting the clinical utility of Cer d18:1/18:0 in stratifying patients with risk of type 2 diabetes.[6] CerS2 produces ceramides with very long C_{24}- and C_{22}-fatty acyl (VLCFA) chains and is particularly active in liver, specifically in hepatocytes,[17] as well as in kidney and adipose tissue. CerS2-deficient mice suffer from severe hepatopathy, with high rates of hepatocyte apoptosis and proliferation, that results

Received 15 May 2021; accepted 8 August 2021;
https://doi.org/10.1016/j.ymthe.2021.08.021.

Correspondence: Christer S. Ejsing, Department of Biochemistry and Molecular Biology, VILLUM Center for Bioanalytical Sciences, University of Southern Denmark, 5230 Odense, Denmark.
E-mail: cse@bmb.sdu.dk

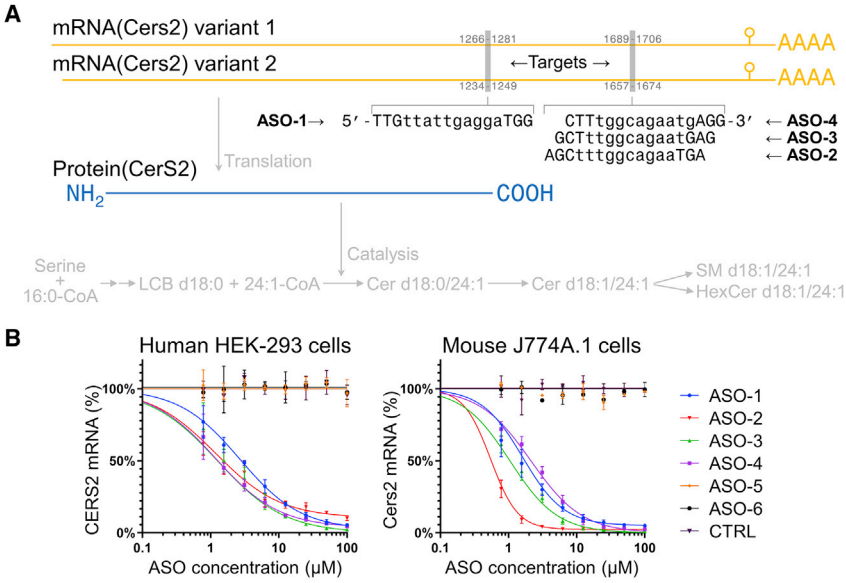

C

Target	ASO	Sequence (5'- 3')	IC_{50} (μM) in HEK-293	IC_{50} (μM) in J774A.1
Cers2	ASO-1	$T_sT_sG_st_st_sa_st_st_sg_sa_sg_sg_sa_sT_sG_sG$	2.6 ± 0.4	1.4 ± 0.4
Cers2	ASO-2	$A_sG_s{}^mC_st_st_st_sg_sg_sc_sa_sg_sa_sa_sT_sG_sA$	1.3 ± 0.5	0.5 ± 0.1
Cers2	ASO-3	$G_s{}^mC_sT_st_st_sg_sg_sc_sa_sg_sa_sa_st_sG_sA_sG$	1.6 ± 0.7	1.2 ± 0.2
Cers2	ASO-4	$^mC_sT_sT_st_sg_sg_sc_sa_sg_sa_sa_st_sg_sA_sG_sG$	1.2 ± 0.2	2.2 ± 0.3
Neg. CTRL	ASO-5	$T_sG_sA_sT_sa_sa_sg_sa_sc_sa_st_st_sT_sA_sT_sT$	-	-
Neg. CTRL	ASO-6	$^mC_sc_sA_sA_sA_st_sc_st_st_sa_st_sa_sa_st_sa_sA_s{}^mC_st_sA_s{}^mC$	-	-

Figure 1. Development of potent ASOs for silencing human CERS2 and mouse Cers2 expression

(A) Sequences of potent ASOs and locations of their target sequences in mouse Cers2 mRNAs. Capital letters represent LNA nucleosides and lowercase letters represent DNA nucleosides. The corresponding translation into CerS2 protein and its enzymatic function in sphingolipid biosynthesis are indicated. Cer, ceramide; CoA, coenzyme A; HexCer, hexosylceramide; LCB, long-chain base; SM, sphingomyelin. (B) Dose-response curves for ASOs targeting CERS2 transcripts in human HEK293 cells and Cers2 transcripts in mouse J774A.1 cells. Cells were treated with the indicated compounds or phosphate-buffered saline (control [CTRL]) for 3 days. (C) Compound sequences and IC_{50} values for the ASOs assayed in HEK293 and J774A.1 cells. Capital letter represents an LNA nucleoside; a lowercase letter represents a DNA nucleoside; superscript m represents a 5-methyl cytosine; a subscript s represents a phosphorothioate internucleoside linkage. Data represent mean ± SD of three independent experiments.

in hepatomegaly and hepatocellular carcinoma.[18–20] Moreover, Cers2 null mice exhibit glucose intolerance due to decreased insulin receptor activation.[21] Notably, several single-nucleotide polymorphisms in the human CERS2 gene are associated with cardiometabolic disease traits, including elevated glycosylated hemoglobin level as well as impaired glomerular filtration rate.[22–26] CerS5 and CerS6 mediate production of primarily C_{16}-ceramides in liver and many other tissues. Notably, both CerS5- and CerS6-derived Cer d18:1/16:0 have been linked to the pathophysiology of insulin resistance showcased by attenuated weight gain of gene-deficient mice,[27,28] possibly through a molecular mechanism that abates fatty acid-induced mitochondrial fragmentation and metabolic dysregulation.[29]

The structure-activity relationships of different ceramides have benefited tremendously from investigations in mouse knockout models. These models have also helped highlight the therapeutic potential of targeting sphingolipid enzymes for the treatment of metabolic disorders, cardiovascular disease, and cancers.[14,30] These models, however, poorly recapitulate clinical settings where healthy individuals, with no apparent genetic deficiencies, develop chronically debilitating metabolic and cardiovascular diseases over a long time period through sedentary lifestyles and poor dietary habits. The pharmacological toolbox for modulating sphingolipid metabolism in this setting has until recently been limited to chemical inhibitors that prompt global and unspecific inhibition of sphingolipid enzymes leading to adverse side effects, especially for the treatment of chronic disorders.[14] An alternative avenue is to use antisense oligonucleotide (ASO)-based gene expression inhibitors.[31] In fact, several validated antisense therapeutics have been designed to specifically target lipid metabolic processes, including apolipoprotein B (APOB),[32] lipoprotein(a),[33] proprotein convertase subtilisin/kexin type 9 (PCSK9),[34] phosphatase and tensin homolog (PTEN),[35] and sterol regulatory element-binding protein 1 (SREBF1).[36,37] For precision treatment of severe diseases with hepatic origin, ASOs can be coupled to *N*-acetylgalactosamine (GalNAc) to enhance hepatocyte-targeted delivery,[38–40] which in turn can mitigate potential nephrotoxic side effects of unconjugated analogs.[41,42] Notably, an unconjugated ASO targeting Cers6 in mice was recently reported to ameliorate metabolic abnormalities in obese mice.[43]

In this study, we outline the development and characterization of a potent locked nucleic acid (LNA)-based ASO that targets both human CERS2 and mouse Cers2 mRNA transcripts. We show that this compound, as well as related analogs, efficiently reduces CerS2 protein expression and activity in cultured cells and elicits a specific lowering of VLCFA-containing ceramides and a compensatory increase in ceramides with shorter chain lengths, including Cer d18:1/16:0. We go on to demonstrate that GalNAc conjugation facilitates specific reduction of CERS2 expression in hepatocytes and that low-dose treatment of mice with this compound prompts specific lowering of CerS2 activity in the liver as well as VLCFA-containing ceramides and other sphingolipids without adverse side effects. Intriguingly, we find that the hepatocyte-specific reduction of CerS2 activity also triggers a parallel modulation of the ceramide molecular profile in the circulation,

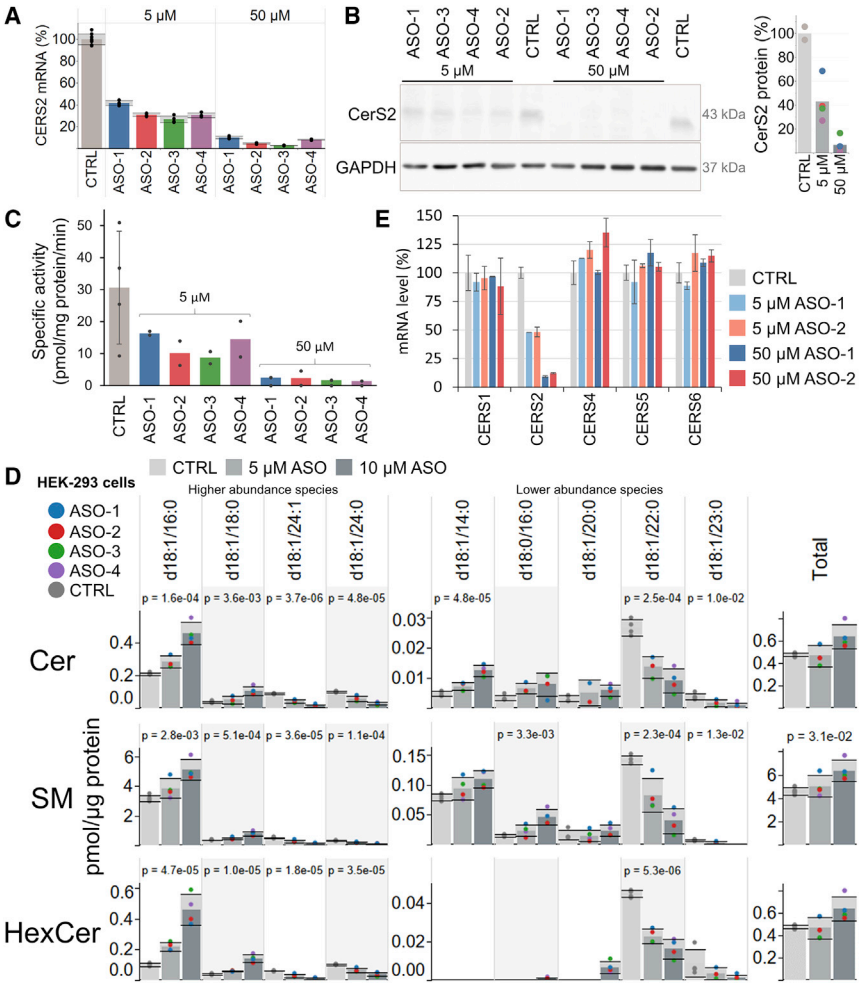

Figure 2. Silencing of CERS2 reduces CerS2 protein expression and activity

(A) CERS2 transcript level in HEK293 cells treated with ASOs at 5 and 50 μM or phosphate-buffered saline (CTRL) for 6 days. Data represent mean ± SD (n = 3 independent experiments) and dots show values of individual treatments. (B) CerS2 protein level in HEK293 cells treated with ASOs at 5 and 50 μM or phosphate-buffered saline (CTRL) for 6 days. Equal protein amounts were separated by SDS-PAGE and analyzed by immunoblotting with antibodies to CerS2 and GAPDH (left panel). Protein abundance (right panel) was determined by densitometry and the CerS2 level is expressed relative to the mean of the control treatments. Data represent mean (n = 2–4 independent experiments) and dots show values of individual treatments. (C) Specific CerS2 activity in HEK293 cells treated with ASOs. CerS2 activity was determined via production of fluorescently labeled 24:1-containing dihydroceramide using cell homogenates, thin-layer chromatography, and densitometry. Data represent mean ± SD (n = 4 independent experiments) and dots show values for individual treatments. (D) Sphingolipid levels in HEK293 cells treated with ASOs or phosphate-buffered saline (CTRL) for 6 days. Data represent mean ± SD (n = 2–4 independent experiments) and dots show values of individual treatments. Significant differences ($p < 0.05$) are highlighted by p value computed using ANOVA. (E) Transcript levels of indicated CERSs in HEK293 cells treated with ASO-1 and ASO-2 for 6 days. Data represent mean ± SD of two independent experiments. See also Figure S1.

demonstrating that the levels of high-risk CVD death marker Cer d18:1/24:1 as well as the protective marker Cer d18:1/24:0 are governed by ceramide biosynthesis in hepatocytes *in vivo*. Overall, our study showcases a therapeutic framework that can be engineered to target any subset of the sphingolipid enzymatic machinery, specifically in hepatocytes *in vivo*, to support both fundamental studies of sphingolipids in disease causality and exploration of the therapeutic utility of targeting ceramide enzymes in the treatment of metabolic and cardiovascular conditions.

RESULTS

Development of potent ASOs for silencing CERS2 expression

To develop a potent antisense inhibitor capable of reducing CerS2 activity, we synthesized a library of LNA-based ASOs that target only conserved sequences in human CERS2 mRNA and mouse Cers2 mRNA (100% homology) and have no match to any other mRNA sequences in the human transcriptome (<0.01% sequence homology). The efficacy of these ASOs was evaluated using a panel of human and mouse cell lines. These cell lines were incubated with ASOs for gymnotic uptake,[44] and the levels of human CERS2 or mouse Cers2 transcripts were measured by quantitative PCR (qPCR) (data not shown). This gave rise to four potent ASOs that were selected for further characterization (Figure 1A).

These ASOs were subsequently assayed for their half-maximal inhibitory concentration (IC_{50}) for silencing CERS2 mRNA expression in human HEK293 cells and in mouse J774A.1 cells. This demonstrated that all four ASOs display a characteristic pharmacological profile with a dose-dependent reduction of transcript levels and potencies in the low micromolar range (Figures 1B and 1C).

Potent ASOs reduce CerS2 activity

Having confirmed target engagement, we next examined the ability of the ASOs to reduce CerS2 protein expression and activity, since this is a major premise for their therapeutic utility. To this end, we treated HEK293 cells with the four ASOs at 5 and 50 μM. Subsequently, we assayed in parallel CERS2 mRNA expression, CerS2 protein expression, and enzyme activity. This recapitulated that treatment with 5 and 50 μM ASO reduces CERS2 expression in a dose-dependent manner to 32% and 6%, respectively, of its level in untreated control cells (Figure 2A). Concomitantly, this prompts a reduction in the CerS2 protein level to 43% and 7%, respectively (Figure 2B). Importantly, the ASOs also evoke a pronounced, dose-dependent reduction

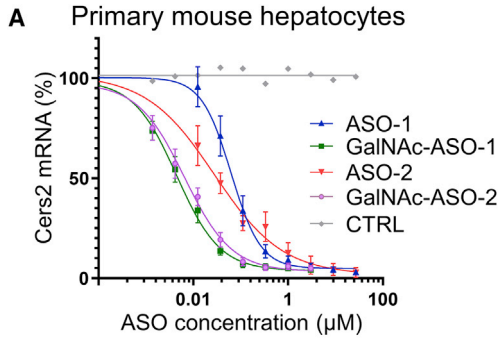

B

ASO	IC_{50} (nM)
ASO-1	63 ± 15
GalNAc-ASO-1	5 ± 2
ASO-2	27 ± 11
GalNAc-ASO-2	6 ± 2

Figure 3. Improved potency of GalNAc-conjugated ASOs toward silencing Cers2 mRNA

(A) Dose-response curves for ASOs targeting Cers2 transcripts in primary mouse hepatocytes. Cells were treated with the indicated compounds or phosphate-buffered saline (CTRL) for 3 days. Data represent mean ± SD of four independent experiments. (B) IC_{50} values are displayed as mean ± SD of four biological replicates.

in CerS2 activity to 20% and 5%, respectively (Figure 2C). Taken together, these data demonstrate that all four ASOs are not only capable of efficiently lowering the CERS2 transcript level but also the CerS2 protein and its enzymatic activity.

To explore whether reducing CerS2 expression also modulates levels of ceramides and downstream metabolically connected sphingolipids, we analyzed ASO-treated HEK293 cells by in-depth MS^{ALL} lipidomics (Table S1). Notably, MS^{ALL} analysis is a lipidomics technology that affords high-fidelity identification and accurate quantification of molecular lipid species at a lipidome-wide level using high-resolution tandem mass spectrometry (MS/MS).[45,46] This analysis demonstrated a dose-dependent reduction in CerS2-specific ceramide products with VLCFAs, including Cer d18:1/24:1 and Cer d18:1/24:0 (Figure 2D). In addition, we observed an increase in the long-chain fatty acyl (LCFA)-containing ceramides, including Cer d18:1/16:0, Cer d18:1/18:0, and Cer d18:1/14:0. Overall, the total level of ceramides did not change significantly, and the modulation of the ceramide molecular profile is propagated directly into downstream SM and hexosylceramide (HexCer, most likely glucosylceramide) products (Figure 2D). Notably, a similar shift to production of LCFA-containing ceramides has been observed in livers of Cers2 null mice that are practically devoid of Cer d18:1/24:1 and Cer d18:1/24:0.[19]

To examine whether the increase in LCFA-containing ceramides is due to a compensatory increase in the expression of other CerSs we measured their transcript levels. This showed that the expression of CERS1, CERS4, CERS5, and CERS6 do not change upon silencing CERS2 (Figure 2E). These data suggest that the increase in LCFA-containing ceramides is not due to elevated expression of other CerSs with specificities toward LCFA-CoAs. Hence, the accumulation of LCFA-containing ceramides could be due to a buildup of LCFA-CoAs attributed to their ineffective conversion to downstream VLCFA-CoA products and utilization by CerS2. Alternatively, post-translational mechanisms for regulation of enzymatic activity, especially for CerS5 and CerS6, via protein-protein interactions[47] as well as protein phosphorylation[48,49] could be alternative compensatory mechanisms of action.

GalNAc conjugation improves potency of ASOs

Having successfully developed a series of potent LNA-based ASOs that specifically silence CERS2/Cers2 gene expression *in vitro*, we next sought to evaluate their utility for perturbing CerS2 function *in vivo*. A pilot study showed that treating mice with a relatively high dose of ASOs (2.8 μmol/kg, ∼15 mg/kg; five doses across 16 days) rendered up to 90% and 70% reduction of Cers2 expression in both the liver and the kidney, respectively (data not shown). This concurred with 80% and 70% reduction in CerS2 activity in both the liver and the kidney, respectively (data not shown). Moreover, this pilot study revealed that ASO-1 and ASO-2 are more efficacious for pharmaceutical intervention due to lower hepatotoxicity (monitored by serum alanine aminotransferase levels) as compared to ASO-3 and ASO-4 (data not shown). Based on these findings we chose to explore the therapeutic utility of only ASO-1 and ASO-2 in further detail.

To further improve the therapeutic efficacy of ASO-1 and ASO-2 we equipped these compounds with a trivalent GalNAc moiety. Notably, we and others have previously shown that GalNAc conjugation targets RNA therapeutics to hepatocytes via binding to the asialoglycoprotein receptor expressed specifically on the cell surface.[33,39,50] As a first step to determine the efficacy of the GalNAc-conjugated ASOs, we assessed their ability to silence Cers2 mRNA in primary mouse hepatocytes. This assessment confirmed the potency of our unconjugated ASOs toward mouse Cers2 expression with IC_{50} values in the low nanomolar range of 27–63 nM (Figures 3A and 3B). Furthermore, we found that the GalNAc-conjugated analogs also display a characteristic pharmacological profile with dose-dependent reduction of the Cers2 transcript level with up to 13-fold greater potency than the unconjugated analogs (i.e., IC_{50} values of 5–6 nM). Importantly, these data not only underpin the improved efficacy and potency of our GalNAc-conjugated ASOs to lower Cers2 expression specifically in hepatocytes, but they also provide an avenue for further *in vivo* testing at lower doses as compared to treatment with unconjugated ASOs, which have a higher risk of nephrotoxic side effects.

Hepatocyte-specific targeting reduces CerS2 activity in the liver

Next, we reasoned that our more potent GalNAc-conjugated compounds should result in specific delivery to liver tissue *in vivo* and prompt a specific lowering of CerS2 activity and a shift in the molecular profile of ceramides in the liver. To explore this, we carried out a short-term study where mice were treated with equimolar doses (276 nmol/kg; two doses across 7 days) of the unconjugated or the

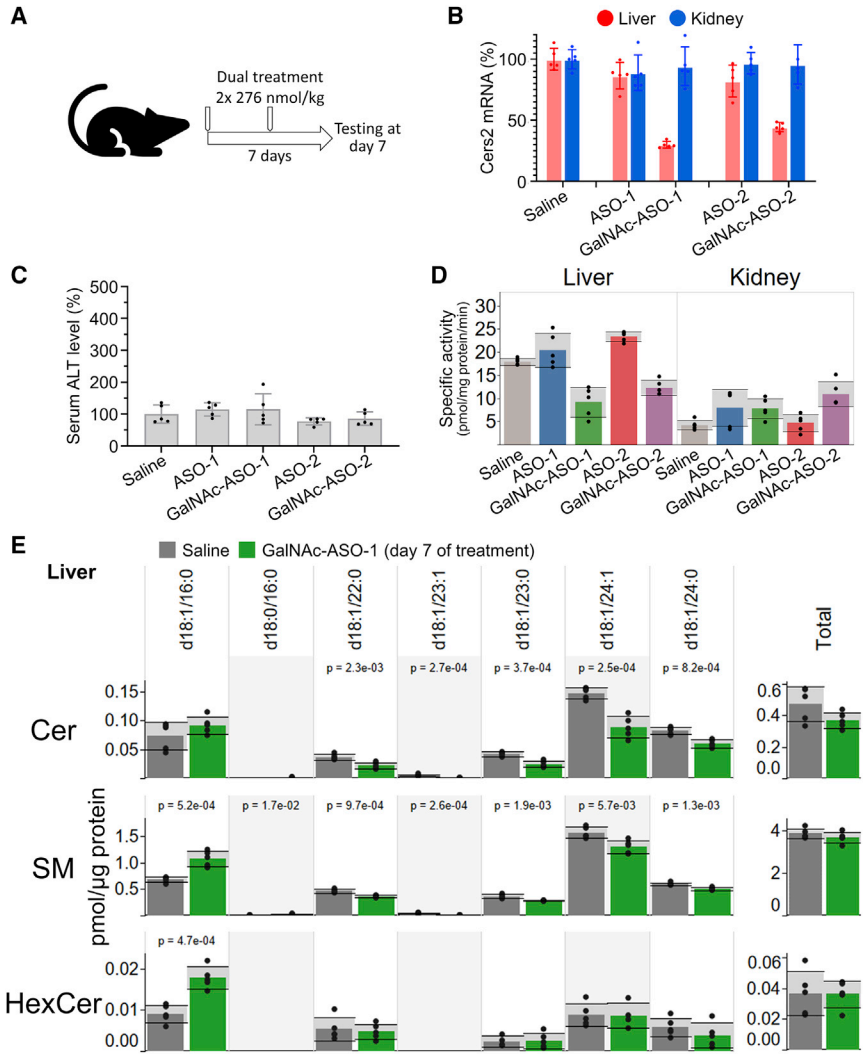

Figure 4. GalNAc-conjugated ASOs prompt specific reduction in liver Cers2 expression and activity in adult animals

(A) Design of short-term *in vivo* study with dual treatments. Ten-week-old C57BL/6J mice were treated twice with ASO-1, GalNAc-ASO-1, ASO-2, or GalNAc-ASO-2 across a 7-day period. The mice were injected on day 0 and 3 with 278 nmol/kg (approximately 2.1 mg/kg and 1.5 mg/kg for GalNAc-ASOs and ASOs, respectively). Control mice were treated with saline. Data in following panels represent mean ± SD and dots show individual measurements (n = 5 biological replicates). (B) Relative expression of Cers2 in liver and kidney. (C) Relative level of alanine aminotransferase (ALT) in serum, a proxy for hepatotoxicity. (D) Specific CerS2 activity in liver and kidney. (E) Sphingolipid levels in livers of mice treated with saline or GalNAc-ASO-1. Significant differences ($p < 0.05$) are highlighted by p value computed using ANOVA.

GalNAc-conjugated ASOs across a 7-day period (Figure 4A). Analysis of transcript levels in liver and kidney demonstrated that the low-dose treatment with unconjugated ASOs does not affect Cers2 expression in either of the two tissues (Figure 4B). Conversely, we found that both GalNAc-ASO-1 and GalNAc-ASO-2 elicit a potent, specific, and significant reduction of the Cers2 transcript level only in the liver to 25% and 45%, respectively. None of the treatments rendered signs of hepatotoxicity (Figure 4C). To confirm that the treatments translate into a reduction of protein function, we assayed CerS2 activity in the liver and kidney. This revealed that only the treatments with the GalNAc-conjugated ASOs, and not the unconjugated ASOs, cause a specific reduction in liver CerS2 activity (Figure 4D).

To further explore the metabolic impact of the hepatocyte-specific Cers2 silencing we carried out MS^{ALL} lipidomics of liver tissue from the saline- and GalNAc-ASO-1-treated mice (Table S2). As expected, the levels of VLCFA-containing ceramides, including Cer d18:1/24:1 and Cer d18:1/24:0, were reduced in livers of mice treated with GalNAc-ASO-1 (Figure 4E). Moreover, we observed an increase in the LCFA-containing Cer d18:1/16:0 species, which maintains the total level of ceramides in the liver constant. Notably, we also found that the characteristic shift in the ceramide molecular profile is propagated into the pools of metabolically coupled SM and HexCer molecules (Figure 4E).

Overall, these data demonstrate that our developed GalNAc-conjugated ASOs facilitate specific downregulation of CerS2 function and activity in the liver, and specifically in hepatocytes. We deem that these ASOs can serve as both tool compounds to investigate the molecular physiology of perturbing CerS2 activity in hepatocytes of adult animals, mitigating confounding effects from developmental compensation in genetically modified animals, as well as exploring the therapeutic utility of targeting Cers2 in models of cardiometabolic disorders. Notably, from hereon we chose to investigate the therapeutic potential of GalNAc-ASO-1 in further detail due to its more potent lowering of Cers2 expression (Figure 4B) as well as its marginally better reduction in CerS2 activity compared to GalNAc-ASO-2 (Figure 4D).

Single low-dose treatment prompts prolonged silencing of liver Cers2 expression

Having established that the GalNAc-conjugated ASOs are effective in specifically lowering CerS2 activity in the liver, we next carried out a duration-of-effect study to determine how long the silencing of Cers2 would have an effect. To this end, mice were treated with a single low-dose of GalNAc-ASO-1 (276 nmol/kg; one dose) (Figure 5A), and the

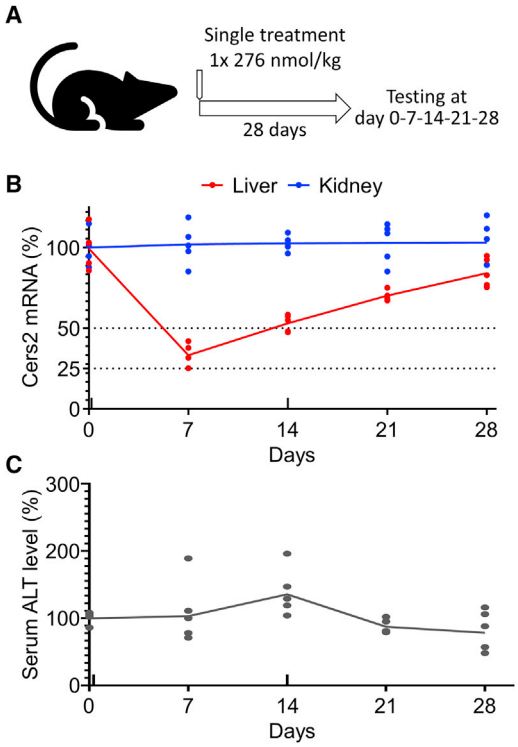

Figure 5. Duration of GalNAc-ASO-1 action after a single low-dose injection in mice

(A) Design of duration of effect study. Ten-week-old mice were treated with a single intravenous injection of GalNAc-ASO-1 (2.1 mg/kg, 0.94 mmol/kg). Mice were euthanized at the indicated time points and tissue samples were collected. Data in the subsequent panels represent mean values ± SD relative to day 0, and dots show values of individual measurements (n = 5 biological replicates). (B) Relative Cers2 transcript level in liver and kidney. (C) Relative level ALT in serum, a proxy for hepatotoxicity.

liver as well as kidney were analyzed for Cers2 expression after 0, 7, 14, 21, and 28 days. This analysis recapitulated our previous finding that GalNAc-ASO-1 specifically targets Cers2 expression in the liver and not in the kidney (Figure 5B). Specifically, 7 days after onset of treatment the level of Cers2 mRNA in liver was reduced to 34% of its initial level. After 14 days, the Cers2 transcript level had reverted back to 53% of its initial level, and after 21 and 28 days the expression continued to gradually approach the initial 100% expression level. Importantly, parallel monitoring of the alanine aminotransferase level in serum again showed no sign of hepatotoxicity across the treatment period (Figure 5C). Based on these data, together with the results of the previously outlined *in vivo* study (Figure 4), we conclude that our GalNAc-ASO-1 compound is well tolerated in mice and has an acceptable safety margin for weekly administration at a low dose.

Long-term silencing of Cers2 prompts minor changes in the liver proteome

Next, we sought to explore the efficacy of our compound for long-term treatment, as this is a major prerequisite for its therapeutic utility in clinical settings. To this end, we carried out a multiple-treatment study with weekly low-dose administration of GalNAc-ASO-1 as well as unconjugated ASO-1 and saline as controls (276 nmol/kg; five doses across 35 days) (Figure 6A). Transcript analysis after 35 days demonstrated that also long-term GalNAc-ASO-1 treatment specifically reduces the Cers2 transcript in liver to 13% of the level in control mice treated with saline (Figure 6B). Moreover, GalNAc-ASO-1 treatment prompts a marginal 14% reduction in the kidney Cers2 transcript level, which is similar to the minor effects of the unconjugated ASO-1 in liver and kidney following long-term treatment.

To verify that the long-term treatment mediates a concomitant reduction in CerS2 protein expression, and to explore more broadly how this impinges on liver physiology, we carried out a quantitative proteomics analysis of liver tissue from the mice treated with GalNAc-ASO-1 and saline. This analysis quantified 5,534 proteins (Table S3) having an average biological variation of only 6.5% (Figure S2). This latter metric demonstrates that our protein quantification is highly precise at the proteome-wide level and that subtle differences are more likely to be statistically significant. Surprisingly, we found that the GalNAc-ASO-1 treatment produces only a minor remodeling of the liver proteome with 96 proteins showing significant differences in abundance ($q < 0.05$ and fold change greater than 1.5) (Figure 6C). Of these proteins, 72 and 24 were upregulated and downregulated, respectively. Among the most downregulated proteins, we found CerS2, having an expression level that is 14% of its level in saline-treated control mice (Figures 6C and 6D).

To examine whether the altered protein expression is primarily due to the reduction of CerS2 activity or potential off-target effects of the GalNAc-ASO-1 compound, we compared our protein data with transcriptomics data from livers of Cers2 null mice.[20] This analysis revealed that most of the 96 differentially expressed proteins have a matching differentially regulated mRNA in Cers2$^{-/-}$ mice. Specifically, 46 (64%) of the 72 upregulated proteins have a matching upregulated transcript, whereas 8 (33%) of the 24 downregulated proteins have a matching downregulated transcript. This high similarity between transcript and protein levels strongly suggests that the minor alteration in liver protein expression following the long-term GalNAc-ASO-1 treatment is largely a bona fide phenotypic consequence of reduced CerS2 activity rather than off-target effects of the ASO compound.

Finally, we explored the metabolic consequences of the hepatocyte-specific reduction of CerS2 activity by interrogating the proteomics data for differential expression of sphingolipid enzymes (e.g., Sptlc1) and related proteins (e.g., Ormdl3). This showed identification of 13 proteins involved in sphingolipid homeostasis, whereof 7 are differentially expressed (Figure 6D). Among three downregulated proteins we found CerS2 ($q = 5e{-}8$), glucosylceramidase Glcm ($q = 0.02$), and galactocerebrosidase Galc ($q = 0.06$), with the latter two being involved in turnover of glycosphingolipids. Among five upregulated proteins we found sphingosine-1-phosphate phosphatase 1 (Sgpp1, $q = 0.006$) involved in dephosphorylation of long-chain base

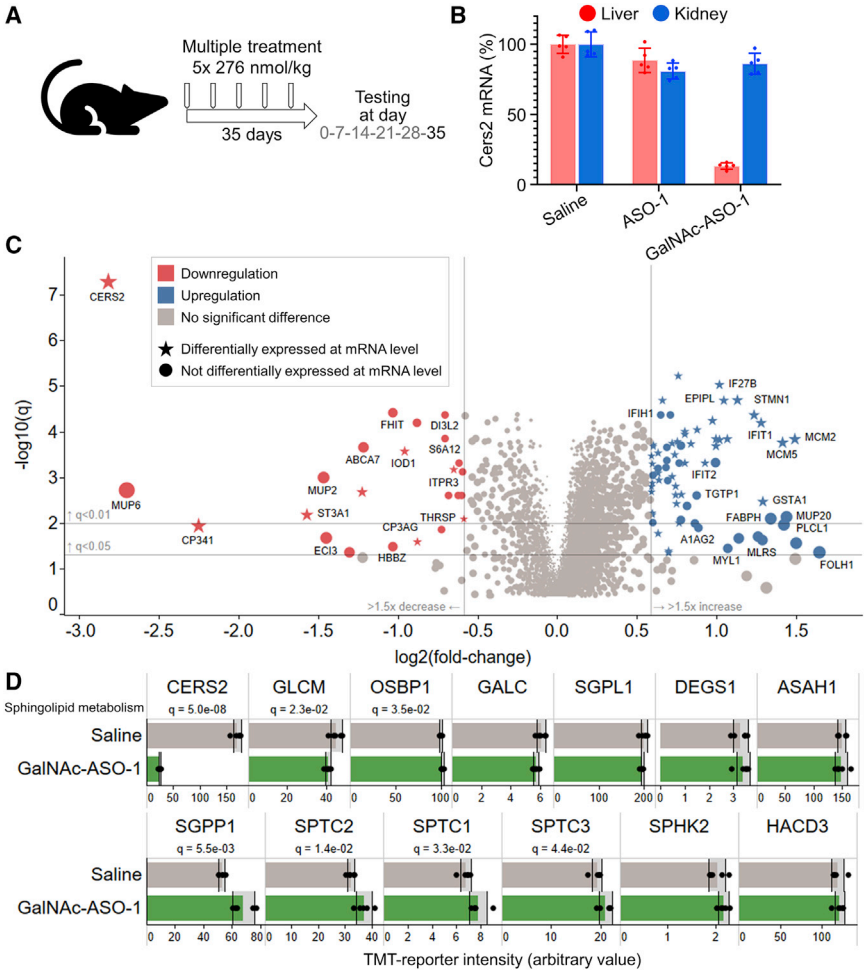

Figure 6. Minimal proteome remodeling upon long-term, hepatocyte-specific Cers2 silencing

(A) Design of long-term study with multiple treatments. Ten-week-old mice were treated weekly with GalNAc-ASO-1 or ASO-1 across a 35-day period. The mice were injected intravenously on days 0, 7, 14, 21, and 28 with 278 nmol/kg (2.1 mg/kg and 1.5 mg/kg for GalNAc-ASO-1 and ASO-1, respectively). Control mice were treated with saline. Blood plasma was collected prior to each dosing at days 0, 7, 14, 21, and 28 (indicated in gray), and the mice were euthanized on day 35 followed by collection of blood plasma, liver, and kidney. (B) Relative Cers2 transcript levels in liver and kidney at day 35 after onset of treatment. Data represent mean ± SD and dots show individual treatments (n = 5 biological replicates). (C) Volcano plot depicting differences in liver protein expression between GalNAc-ASO-1- and saline-treated mice. Protein expression data are correlated to transcriptomics data from Pewzner-Jung et al.[20] (D) Expression levels of sphingolipid metabolic machinery in liver. Data represent average reporter intensity (arbitrary unit) ± SD (n = 5 biological replicates) and dots show values of individual replicates. Significant differences ($q < 0.05$) are highlighted by computed q values. See also Figure S2.

phosphates and production of long-chain bases (including sphingosine and sphinganine), and all three members of the serine palmitoyltransferase family, Sptlc1 (q = 0.03), Sptlc2 (q = 0.01), and Sptlc3 (q = 0.04), responsible for biosynthesis of long-chain bases. These findings indicate that lowering CerS2 activity triggers a broader repertoire of compensatory responses that serve to maintain sphingolipid homeostasis by increasing the biosynthesis of long-chain bases (mediated by Sptlc1/2/3 and Sgpp1) and minimizes activities that lead to futile degradation of glycosphingolipids (mediated by Glcm and Galc).

Hepatocyte-specific silencing of Cers2 prompts remodeling of circulating ceramides

To verify that the long-term treatment also translates into a lowering of CerS2-specific ceramides, we carried out MS^{ALL} lipidomics of liver tissue from the mice treated with GalNAc-ASO-1 and saline (Table S4). This analysis verified that the hepatocyte-specific silencing of Cers2 lowers the absolute levels of VLCFA-containing ceramides, including Cer d18:1/24:1 and Cer d18:1/24:0 (Figure 7A). Notably, this reduction was accompanied by a significant increase in Cer d18:1/16:0 and its biosynthetic precursor Cer d18:0/16:0. This compensatory effect, however, does not add up to maintain a constant total ceramide level, as observed for treated HEK293 cells (Figure 2D), in livers of mice subjected to short-term GalNAc-ASO-1 treatment (Figure 4E) and livers of Cers2 null mice.[19] Moreover, the characteristic shift in the ceramide molecular profile is again propagated into metabolically connected SM and HexCer molecules (Figures 7A and S3A). Notably, the specific silencing of Cers2 evokes no evident lipid metabolic off-target effects, evidenced by no major changes of the overall FA profile in the liver (Figure S4A) or that of key enzymatic machinery involved in FA metabolism (Figure S4B). Based on these findings we conclude that the long-term treatment translates into effective lowering of VLCFA-containing ceramides in the liver by specifically impairing CerS2 function in hepatocytes.

Finally, we examined the therapeutic utility of Cers2 targeting in reference to modulating levels of plasma ceramide biomarkers associated CVD death. To this end, we carried out MS^{ALL} lipidomics of blood plasma collected across six time points during the 35-day treatment period (Table S5). Intriguingly, this demonstrated a progressive lowering of CerS2-related ceramides, including Cer d18:1/24:1 and Cer d18:1/24:0, until day 21, after which the levels of VLCFA-containing ceramides became slightly elevated again (Figure 7B). In comparison, the plasma level of Cer d18:1/16:0 was only marginally modulated (p = 0.053) across the 35-day treatment period, with a minor elevation until day 14, after which the level declined again. Furthermore, the systematic shifts in ceramide molecular profile are directly propagated into the pools of plasma SM and HexCer molecules, with the molecular

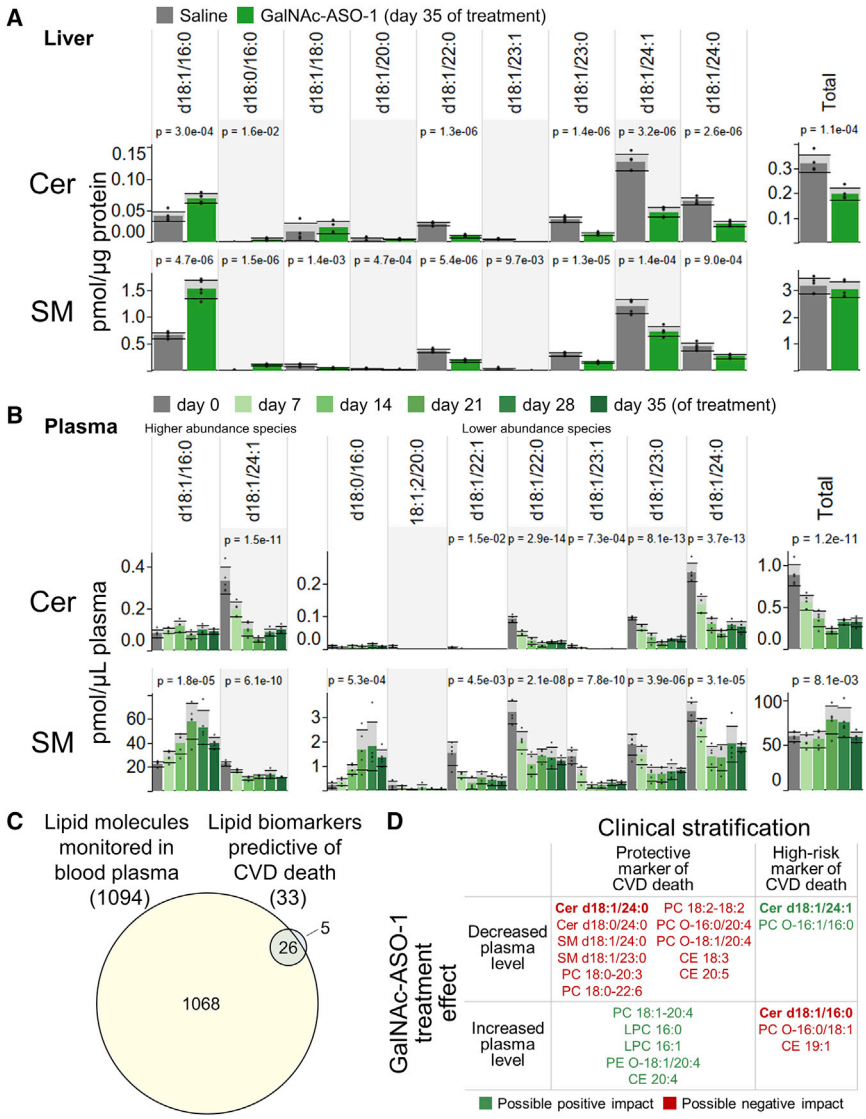

Figure 7. Hepatocyte-specific silencing of Cers2 modulates levels of circulating ceramides

Ten-week-old mice were treated with GalNAc-ASO-1 or saline as outlined in Figure 6A. Data in (A) and (B) represent mean ± SD and dots show individual treatments (n = 5 biological replicates). Significant differences ($p < 0.05$) are highlighted by p value computed using ANOVA. CE, cholesteryl ester; LPC, lysophosphatidylcholine; PC, phosphatidylcholine; PC O-, ether-linked phosphatidylcholine; PE, phosphatidylethanolamine. (A) Level of ceramide and sphingomyelin molecules in liver after the 35-day treatment period. (B) Concentration of ceramide and sphingomyelin molecules in blood plasma of mice treated with GalNAc-ASO-1 across the indicated time period. (C) Venn diagram of lipid molecules monitored in plasma in the current study and lipids associated with fatal outcome of coronary artery disease.[4] (D) Relationship between risk stratification and lipid biomarkers that are significantly changed by GalNAc-ASO-1 treatment ($p < 0.1$). See also Figures S3 and S4.

hallmark that 16:0-containing SM and HexCer species become significantly elevated until day 21 and are then reduced again (Figures 7B and S3B). Taken together, these findings demonstrate a direct metabolic coupling between ceramide biosynthesis in hepatocytes and the levels of circulating ceramide molecules, especially the CerS2-specific VLCFA-containing ceramides. Moreover, the data also indicate that adolescent mice subjected to long-term the GalNAc-ASO-1 treatment undergo an adaptation between day 21 and 28 that serves to attenuate the reduced level of VLCFA-containing ceramides and metabolically coupled sphingolipids. Notably, future studies should be carried out to explore the molecular and functional underpinnings of this finding in further detail.

Lastly, we explored the broader pharmacological potential of the GalNAc-ASO-1 treatment by assessing its impact across the panel of all CVD death-related lipids. Notably, the original study leading to the discovery of the ceramide biomarkers reported a total of 31 lipids to be risk markers of a fatal outcome in patients with coronary artery disease.[4] Querying our comprehensive lipidomics data revealed specific detection of 25 of these plasma lipids (Figure 7C), of which 21 are significantly modulated by the GalNAc-ASO-1 treatment. Compared to clinical risk stratification, we found that the plasma levels of 7 of these lipids are favorably modulated by treatment whereas 14 are unfavorably modulated (Figure 7D). Among the favorably modulated lipids is the specific lowering of the CerS2-related high-risk marker Cer d18:1/24:1 as well as elevation of the protective markers LPC 16:0, LPC 16:1, PC 18:1-20:4, PE O-18:1/20:4, and CE 20:4, where the latter three have an ω-6-arachidonyl chain feature (i.e., 20:4). Among the unfavorably modulated lipids is the lowering of the CerS2-related protective markers Cer d18:1/24:0, SM d18:1/24:0, and SM d18:1/23:0, and several protective markers with ω-3 chain features, including PC 18:0-22:6, PC 18:0-20:3, CE 18:3, and CE 20:5, as well as a minor elevation of the high-risk marker Cer d18:1/16:0. In the context of therapeutically modulating the risk of CVD death, these data demonstrate that the Cers2 targeting is highly effective in lowering the high-risk CVD death marker Cer d18:1/24:1, but that this also prompts, at least in healthy adolescent mice, the inadvertent lowering of several protective sphingolipid markers with saturated VLCFA chains as well as several protective lipids with ω-3 FA chain features.

DISCUSSION

The recent discovery of bona fide ceramide biomarkers prognostic of CVD death has prompted a profound interest in understanding the

molecular basis of its causality and devising pharmaceutical strategies for targeting ceramide biosynthesis that ideally mitigate the risk of death for individuals with CVD. In this study, we set out to explore the therapeutic potential of targeting CERS2 as an avenue to lower the high-risk biomarker Cer d18:1/24:1 in the circulation. To this end, we developed a potent and specific LNA-based ASO capable of silencing both human CERS2 and mouse Cers2 expression, specifically in hepatocytes *in vivo* when tethered to a GalNAc-based drug delivery system. We show that our ASO compound not only silences the mRNA level but also reduces CerS2 protein expression and enzyme activity, both *in vitro* and *in vivo*. We go on to show that our compound reduces the biosynthesis of VLCFA-containing ceramides in the liver of mice and that this evokes a direct lowering of VLCFA-containing ceramides in the circulation, including the high-risk biomarker Cer d18:1/24:1 as well as other sphingolipids. Furthermore, we show that our ASO compound is well tolerated in mice and only elicits a minor remodeling of the liver proteome that primarily reflects the reduced CerS2 expression and levels of VLCFA-containing sphingolipids. Overall, our study showcases a therapeutic framework that can be engineered to target any subset of the sphingolipid enzymatic machinery, specifically in hepatocytes *in vivo*. This framework can support fundamental studies of sphingolipids in disease causality and serve as a stepping stone to explore the therapeutic utility of targeting ceramide enzymes in rodent models of metabolic and cardiovascular disease.

Although our ASO compound is potent, specific, and has no apparent side effects when administrated at a low dose, we find that its utility for modulating the high-risk biomarker Cer d18:1/24:1 is seemingly jeopardized by the inadvertent reduction of several protective sphingolipid markers with saturated VLCFAs, especially Cer d18:1/24:0. This effect is readily explained by the substrate specificity of CerS2, which uses fatty acyl-CoAs with saturated and monounsaturated chains having between 20 and 24 carbon atoms.[13,14] Hence, in light of the CerS2 substrate specificity, it appears that pharmacological targeting of CERS2 to mitigate the risk of death in patients with CVD will be challenging since it is likely to reduce both the high-risk biomarker Cer d18:1/24:1 as well as the protective biomarker Cer d18:1/24:0. Notably, also the ceramide ratios Cer d18:1/24:1-to-Cer d18:1/24:0 and Cer d18:1/16:0-to-Cer d18:1/24:0 have been reported to be high-risk biomarkers of CVD death, with even better predictive powers than the levels of the individual plasma ceramides.[4,5] In this context, we find that the treatment with GalNAc-ASO-1 does not affect the high-risk marker Cer d18:1/24:1-to-Cer d18:1/24:0 considerably, but it does inadvertently elevate the high-risk marker Cer d18:1/16:0-to-Cer d18:1/24:0 by up to 4.7-fold (Figure S3C). Nevertheless, despite these seemingly unfavorable effects of CERS2 targeting, we deem that further investigation using rodent models of metabolic and cardiovascular disease, such as atherosclerosis-prone apolipoprotein E-deficient mice, are warranted to fully explore the potential of the ASO compound. Such studies could lead to the development of specialized therapeutic modalities, including combination therapies, that eventually translate into lowered CVD death risk for individual patients as well as combating the enormous socioeconomic burden of CVD and its comorbidities at the society level.

Our study not only provides a better understanding of the challenges associated with pharmacological targeting CERS2 but also gives fundamental understanding into the metabolic origin of the ceramide biomarkers and their metabolic coupling to other risk-associated (sphingo)lipids. Importantly, our data uncover that hepatocytes are major determinants of the high-risk ceramide biomarkers Cer d18:1/24:1 and Cer d18:1/16:0 as well as the protective biomarker Cer d18:1/24:0. By the use of our hepatocyte-specific GalNAc-ASO-1 compound and comprehensive MS^{ALL} lipidomics analysis, we elucidate that this regulation is governed at the level of ceramide biosynthesis and that this goes beyond the three ceramide biomarkers to also include downstream metabolically connected SM and HexCer molecules, which were originally also stratified as risk-associated lipids.[4] Importantly, this insight strongly suggests that the molecular etiology of CVD death does not only involve the three ceramide biomarkers, but rather a more intricate metabolic network of enzymatic transitions and crosstalk between hepatocytes and the circulation. To harness this deeper level of molecular complexity will certainly benefit from the use of more extensive lipidomics technology[46,51] that goes beyond targeted analysis of only the three ceramide biomarkers. Moreover, it will be exciting in future studies to extend this analysis to cover different lipoprotein particles, thereby giving us a more detailed understanding of the molecular relationship between CerS2 activity in hepatocytes and its link to CVD.

In summary, our study highlights the therapeutic utility and challenges of targeting CERS2 for modulating high-risk ceramide biomarkers of CVD death, showcases a generic therapeutic framework for targeted disruption of sphingolipid metabolic machinery specifically in hepatocytes *in vivo*, uncovers that ceramide biosynthesis in hepatocytes plays a central role in controlling the levels of numerous risk-associated sphingolipids in the circulation, and lays the groundwork for exploring the therapeutic efficacy of ASOs toward ceramide biosynthesis in rodent models of metabolic and cardiovascular disease. Furthermore, the large amount of lipidomics and proteomics data collected in this work should be a useful resource for the scientific community to further investigate molecular aspects of ceramide biology that are not covered in this study.

MATERIALS AND METHODS

Chemicals

All chemicals were of high-performance liquid chromatography (HPLC) grade and were purchased from Sigma-Aldrich or VWR, unless stated otherwise. Methanol and chloroform were from BioSolve and Rathburn Chemicals, respectively. Synthetic lipid standards were purchased from Avanti Polar Lipids and Larodan Fine Chemicals.

Oligonucleotide design and synthesis

Single-stranded LNA-based ASOs complementary to human CERS2 mRNA and mouse Cers2 mRNA (ENSG00000143418 and ENSMUSG00000015714) were synthesized using standard phosphoramidite chemistry.[39] DNA phosphoramidites were purchased from Sigma-Aldrich, and LNA phosphoramidites were produced in-house

(albeit LNA oligonucleotides are also commercially available). Aminolinker C6 was purchased from Link Technologies. Unconjugated ASO and 5′-aminolinker C6 precursors (for GalNAc-conjugated ASOs) were synthesized on NittoPhase HL UnyLinker 350 support (Kinovate Life Sciences) on an ÄKTA Oligopilot (GE Healthcare) at a 130 μmol scale. After synthesis, the oligonucleotides were cleaved from the support using aqueous ammonia at 65°C overnight. The oligonucleotides were purified by ion exchange on SuperQ-5PW gel (Tosoh Bioscience) and desalted using a MF-Millipore membrane. After lyophilization, the ASOs were characterized by liquid chromatography (LC)-MS. GalNAc-conjugated ASOs were prepared using GalNAc cluster (GN2) as described in patent application WO 2017/021385 A1 (examples 1–10). The free GalNAc acid was activated using *N*-hydroxysuccinimide and *N*-(3-dimethylaminopropyl)-*N*′-ethylcarbodiimide hydrochloride in a mixture of dimethylformamide and dimethyl sulfoxide, and then added to the 5′-aminolinker C6 precursor (with 3-to-4 molar excess of GN2) in 20 mM sodium hydrogen carbonate together with triethylamine. After ∼12 h, the reaction mixture was applied directly to ion-exchange purification and desalting as described above for the unconjugated ASOs.

Cell culture, ASO treatment, and RNA isolation

Human HEK293 and mouse J744A.1 cells were plated 24 h prior to addition of ASOs, which were dissolved in PBS at the indicated concentrations. After an ASO incubation time of 72 h, cells were lysed and total RNA was extracted using the PureLink Pro 96 RNA purification kit (Thermo Fisher Scientific), and quantitative reverse transcriptase PCR (qRT-PCR) for gene expression analysis was performed as described below. Primary mouse hepatocytes were isolated from C57BL/6 mice by a two-step collagenase liver perfusion method.[52] Freshly isolated hepatocytes were plated in collagen-I-coated 96-well plates at 25,000 cells/well in William's medium E, supplemented with 1× penicillin (Pen)/streptomycin (Strep)/glutamine (Invitrogen) and 10% fetal bovine serum (ATCC). 3 h after plating, the hepatocytes were treated with ASOs at the indicated concentrations for 72 h, followed by RNA extraction and qRT-PCR as described below.

In vivo studies in mice

In vivo studies were conducted in accordance with European standards, the guideline of *Policies Governing the Use of Live Vertebrate Animals* by the University of Tokyo, based on *The Public Health Service Policy on Humane Care and Use of Laboratory Animals* by the Awardee Institution (revised May 1985), and by the National Institutes of Health *Guide for the Care and Use of Laboratory Animals* (revised 1985). Furthermore, protocols were approved by the Danish National Committee for Ethics in Animal Experiments. Inbred C57BL/6JBom female mice weighing 20 ± 2 g (mean ± standard deviation) were obtained from Taconic. The animals were housed in groups of five, and water and a standard diet were supplied *ad libitum*. The vivarium was maintained at a constant temperature (23°C ± 1°C) and humidity (40% ± 5%) under a 12-h light/12-h dark cycle throughout the studies. The treatment groups (n = 5) received either 0.9% saline or saline-formulated ASO administered by intravenous injection. Interim blood samples were drawn from the sublingual vein in K2EDTA tubes, and plasma was prepared by centrifugation (1,500 × *g*, 10 min, 4°C). Mice were anesthetized (using 70% CO_2/30% O_2) before euthanasia by cervical dislocation. Collected samples of plasma, liver, and kidney were snap-frozen in liquid nitrogen and stored at −80°C until further processing. Total RNA from liver and kidney tissues was isolated using the MagNA Pure 96 cellular RNA large volume kit (Roche).

qRT-PCR

For gene expression analysis, one-step qRT-PCR was performed using qScript XLT one-step qRT-PCR ToughMix, low ROX (Quantabio) in a duplex setup using the following Thermo Fisher TaqMan assays: CERS1 (Hs04195319_s1), CERS2 (Hs00604577_m1), CERS3 (Hs00698859_m1), CERS4 (Hs00226114_m1), CERS5 (Hs00332291_m1), and CERS6 (Hs00826756_m1), each normalized to expression of GAPDH (Hs99999905_m1) for the human transcript, and Cers2 (Mm00504086_m1; FAM-MGB), normalized to Gapdh (Mm99999915_g1; VIC-MGB_PL) for the mouse transcript, respectively. All data points were performed in duplicates and IC_{50} values were determined using GraphPad Prism software.

Western blot analysis of CerS2 expression

Western blot analysis of HEK293 cells was performed as previously described.[53] Total protein levels in cell homogenates were measured using the Pierce bicinchoninic acid (BCA) protein assay kit (Thermo Fisher Scientific), followed by SDS-PAGE protein separation, blotting, and visualization by enhanced chemiluminescence. The following antibodies were used: anti-CerS2 (HPA027262, Sigma), anti-GAPDH (sc-25778; Santa Cruz), and horseradish peroxidase-conjugated anti-rabbit (111-035-003, Jackson ImmunoResearch) and anti-mouse antibodies (115-035-003, Jackson ImmunoResearch).

Analysis of CerS2 activity

CerS2 activity was assayed in homogenates of HEK293 cells, mouse liver, and kidney as previously described.[54] Briefly, cell and tissue homogenates (40 μg of total protein) were incubated at 37°C for 25 min with 15 μM NBD sphinganine, 50 μM 24:1-CoA (Avanti Polar Lipids), and 20 μM defatted bovine serum albumin (Sigma-Aldrich). Reactions were terminated by addition of chloroform/methanol (1:2, v/v), and lipids were extracted using the Bligh-Dyer procedure. Lipid extracts were dried under N_2, dissolved in chloroform/methanol (9:1, v/v), and separated by thin-layer chromatography using chloroform/methanol/2 M NH_4OH (40:10:1, v/v/v) as the developing solvent. NBD-labeled lipids were visualized using an Amersham Typhoon 5 biomolecular imager (GE Healthcare) and quantified by ImageQuant TL (GE Healthcare).

MS-based lipidomics

HEK293 cells, liver, and plasma were analyzed by MS^{ALL}-based lipidomics, as described previously.[45,46] In brief, cell and tissue homogenates in 155 mM ammonium formate (Sigma-Aldrich), corresponding to 20 and 10 μg of total protein, respectively, were spiked with internal lipid standards, including Cer d18:1/17:0, SM d18:1/17:0, and GluCer

d18:1/12:0 (Avanti Polar Lipids), and subjected to two-step lipid extraction[55,56] (we note that it is preferable to use stable isotope-labeled standards for every lipid class and molecule, and not odd-chain analogs, as these can be of low abundance in biological matrices). Plasma samples (8 μL) were diluted in 155 mM ammonium formate, spiked with internal lipid standards, Cer d18:1/17:0, SM d18:1/17:0, and GluCer d18:1/12:0, and subjected to two-step lipid extraction. Lipid extracts were subsequently analyzed by high-resolution MS^{ALL} analysis in the positive and negative ion mode using an Orbitrap Fusion Tribrid (Thermo Fisher Scientific) equipped with a robotic nanoflow ion source, TriVersa NanoMate (Advion Biosciences). High-resolution Fourier transform MS (FTMS) spectra were recorded using a maximum injection time of 100 ms, automated gain control at 1e5, three microscans, and a target resolution of 500,000. $FTMS^2$ spectra were recorded using a maximum injection time of 100 ms, automated gain control at 5e4, three microscans, a target resolution of 30,000, HCD fragmentation, a quadrupole ion isolation width of 1.0 atomic mass units (amu), and collision energies optimized for individual lipid classes.[45]

Lipid nomenclature

Lipid classes are denoted by their class abbreviations.[57–59] For lipids reported at the "species level," the combined numbers of carbons, double bonds, and hydroxyl groups in the hydrocarbon chains are indicated after the lipid class abbreviation. For example, "PE 38:4" denotes a PE lipid with 38 carbons and 4 double bonds spread across both individual FA chains. For lipids reported at the "molecular species level" (i.e., identification of individual FA chain compositions), individual hydrocarbon chains are indicated in the format of "total number of carbons/number of double bonds," with individual FAs separated by a dash for glycerolipids and glycerolipids. For example, "SM 18:1;2/16:0" indicates a SM lipid containing a C_{18}-sphingosine chain having one double bond and two hydroxyl groups (i.e., 18:1;2) and an amide-linked 16:0 FA chain. For ether lipids, ether-bound hydrocarbon chains are preceded with an "O-," indicating either 1-*O*-alkyl ether or 1-*O*-alkenyl ether (plasmalogen) linkage. For example, PE O-18:1/20:4 is a PE O- lipid with a 20:4 FA chain and an 18-carbon ether-linked chain with one double bond. The double bond could be either that of a 1-*O*-alkenyl ether or positioned along the remainder of the FA chain as a 1-*O*-alkyl ether. We note that exact *sn*- positions and locations of double bonds of individual FAs are not resolved by the applied lipidomics technology.

Lipid abundances from mass spectrometric data

Identification and quantification of lipid molecules was done using the $ALEX^{123}$ and auxiliary data processing pipelines in SAS 9.4 (SAS Institute).[45,59–61] Briefly, lipid molecules detected by full-scan FTMS were identified using a maximum *m/z* tolerance of ±0.0040 amu, corrected for potential ^{13}C isotope interference, required to have a relative detection frequency greater than 0.66 (equivalent to being detected in 66% of all biological replicates for a given sample group) and reported at the species level. Lipid fragment ions detected by FTMS2 were identified using a maximum *m/z* tolerance of ±0.0065 amu, required to have a relative detection frequency greater than 0.66 (equivalent to being detected in 66% of all biological replicates in a given sample group), and reported as molecular lipid species-specific fragments (MLFs) or lipid class-specific fragments (LCFs).[59,61] For high-confidence identification of lipids reported at the species level (e.g., SM 34:1;2), at least one confirmatory LCF detected by FTMS2 was required. For high-confidence identification of molecular lipid species identified by detection of MLFs, the following criteria were set: (1) asymmetric molecular lipid species must be detected by at least a complementary pairs of MLFs (except for protonated PE O species that do not release abundant complementary MLFs); (2) the molecular lipid species must have an ALEX score >0.5 (calculated as the number of detected MLFs relative to the total number of MLFs available in the $ALEX^{123}$ database) or an ALEX score $\leq$0.5 but with detection of >2 MLFs (with the exception that protonated PE O species could be detected by at least 2 MLFs); and (3) confirmation by detection of the corresponding lipid molecule at the species level by full-scan FTMS1 analysis. Identified lipid molecules were quantified by normalizing their intensities to those of respective internal lipid standards, subsequent multiplication by the amount of the respective lipid standard, and normalization to the extracted sample amount (i.e., μg of protein or μL of plasma). Visual inspection of data quality and lipidome features was done using Tableau desktop (Tableau Software).

Sample preparation for proteomics analysis

Samples of liver tissue (~15 mg of tissue per 1 mL of buffer) were mixed with 90°C buffer containing 100 mM triethylammonium bicarbonate as well as 1 mM $MgCl_2$ (Sigma-Aldrich) and homogenized using an Ultra-Turrax (IKA). This was followed by incubation at 80°C for 5 min, cooling to 4°C on ice, 5 min of treatment with 5 U of Benzonase nuclease (Sigma-Aldrich), and taking an aliquot for total protein determination using the Pierce BCA protein assay kit. Homogenates corresponding to ~200 μg of total protein were aliquoted and mixed with protein lysis-reduction-alkylation buffer yielding a final concentration of 1% sodium deoxycholate, 10 mM tris(2-carboxyethyl)phosphine, and 40 mM 2-chloroacetamide (Sigma-Aldrich). Samples were then sonicated using a Bioruptor UCD-200 system (Diagenode) at 4°C for 10 min with 30-s on/off cycles. Next, cysteine reduction and alkylation were carried out by incubating the homogenates for 10 min at 80°C, followed by addition of 4 μg of LysC endoproteinase (Fujifilm Wako Chemicals) and incubation at 37°C for 3 h. Then, 2 μg of trypsin was added and the incubation at 37°C was continued overnight. On the next day the sodium deoxycholate was removed by acidification using trifluoroacetic acid (Sigma-Aldrich) followed by ethyl acetate (Sigma-Aldrich) extraction. Samples were then cleaned by solid phase extraction using HLB cartridges (Waters), according to the manufacturer's protocol. The eluates were dried in a SpeedVac, and the peptides were dissolved in 100 mM 4-(2-hydroxyethyl)-1-piperazineethanesulfonic acid (HEPES) buffer (pH 8.5) (Sigma-Aldrich), and an aliquot was taken for total peptide determination using the Pierce BCA protein assay kit. A total amount of 100 μg of peptides from individual samples was isotopically labeled by incubation with 500 μg of TMT (Tandem Mass Tag) (Thermo Fisher Scientific) for 1 h at room temperature,

followed by quenching using hydroxylamine (Sigma-Aldrich) at a final concentration of 0.5%. The individual samples were mixed equally to yield a single 10-plexed TMT-labeled sample.

Fifty μg of the 10-plexed TMT-labeled sample was offline fractionated by high-pH reversed-phase LC using an UltiMate 3000 HPLC system (Thermo Fisher Scientific) fitted with an Acquity CSH C18 column (300 μm × 100 mm; 1.7-μm particle size; Waters), a flow rate of 5 μL/min, and a gradient from 2% to 60% of buffer B in 1 h (where buffer A was 20 mM aqueous ammonium formate [pH 9] and buffer B was 80% [v/v] acetonitrile and 20% [v/v] buffer A). Twenty subfractions were collected (3 min per fraction) and combined into 10 fractions. The fractions were dried in a SpeedVac, and peptides were dissolved in an aqueous solution containing 2% (v/v) acetonitrile and 0.1% (v/v) trifluoroacetic acid.

MS-based proteomics

The 10 fractions were analyzed by LC-MS/MS using an UltiMate 3000 RSLCnano system coupled to a Q Exactive HF mass spectrometer (Thermo Fisher Scientific). The TMT-labeled peptides were loaded on a PepMap 100 C18 precolumn (300 μm × 5 mm; 5-μm particle size; Thermo Fisher Scientific) at 10 μL/min and then transferred to an analytical pulled-emitter column (50 cm × 75 μm), home packed with Inertsil ODS-3 2-μm sorbent (GL Sciences).[62] Peptides were separated with a flow rate of 450 nL/min at 45°C in a home-made column thermostat using a gradient from 4% to 32% buffer B in 2 h (where buffer A was 0.1% [v/v] formic acid in water and buffer B was acetonitrile with 0.1% [v/v] formic acid). MS analysis was carried out in data-dependent acquisition (DDA) mode with survey FTMS1 spectra recorded using a target resolution of 120,000, AGC target of 3e6, maximum injection time of 100 ms, scan range from *m/z* 300 to 2,000, followed by 20 FTMS2 spectra recorded with a target resolution of 60,000, AGC target of 2e5, maximum injection time of 108 ms, quadrupole isolation window of 1.2, fixed first mass at *m/z* 110, collision energy at 30%, and dynamic exclusion for 40 s.

Protein identification and quantification

LC-MS/MS data were analyzed using MaxQuant (version 1.6.0.16).[63] Data files for all fractions were searched together against the mouse UniProt SwissProt database (from March 26, 2018 and containing 16,975 proteins). Parameters in MaxQuant were set to default values, unless stated otherwise. MS and MS/MS search mass tolerances were set at ±20 ppm. Experiment type was set to "Reporter ion MS^2" with PIF (precursor intensity fraction) filtering at 0.75. Carbamidomethylation of cysteine was selected as a fixed modification, and methionine oxidation and protein N-terminal acetylation were selected as variable modifications. Digestion was set to "Trypsin/P specificity" with a maximum of two missed cleavages. Decoy mode was set to revert. Contaminants were included in the search space. Peptide-spectrum match (PSM) and protein false discovery rate (FDR) were both set at 1%. Identified protein groups were quantified based on their MS/MS reporter ion signal intensity/noise (S/N) values for protein group-specific and unique razor peptides with a label minimum ratio count of 2 required for valid protein group quantification. Assessment of protein expression levels was done using "Reporter intensity corrected" values provided by MaxQuant in the proteinGroups.txt result file. Sample-to-sample normalization was done based on the sum of reporter intensity corrected values for all protein groups for each sample. The LC-MS/MS data and MaxQuant analysis results are deposited in the PRIDE database and can be accessed using the accession number PXD025957.

Statistical analysis and bioinformatics

All data are shown as mean ± standard error. Statistical analysis of lipidomics data was done by analysis of variance (ANOVA) using SAS 9.4 (SAS Institute). Lipid molecules with p values less than 0.05 are considered statistically significant. Statistical analysis of proteomics data was performed with a moderated unpaired t test using the eBayes module in the limma R package.[64] The resulting p values are corrected for multiple hypothesis testing by calculating q values to estimate the FDR. A q value less than 0.05 is considered statistically significant.

SUPPLEMENTAL INFORMATION

Supplemental information can be found online at https://doi.org/10.1016/j.ymthe.2021.08.021.

ACKNOWLEDGMENTS

We thank Reijo Laaksonen, Kim Ekroos, Robin Klemm, Giora Volpert, and members of the Athero-Flux Consortium for constructive comments. This work was supported by funding from the European Union Seventh Framework Programme (FP7-2007-2013) under grant agreement "HEALTH-F2-2013-602222 (Athero-Flux)" (to O.N.J. and C.S.E.). This work was also supported by the Danish Council for Strategic Research (11-116196, to C.S.E.), the University of Southern Denmark (SDU2020, to C.S.E.), the Lundbeckfonden (R54-A5858, to C.S.E.), and the VILLUM Center for Bioanalytical Sciences (VKR023179, to O.N.J. and C.S.E.).

AUTHOR CONTRIBUTIONS

S.S., A.H.F., M.W.L., and C.S.E. conceived and designed the study. S.S., S.F.G., I.D.Z., S.K., N.A., R.R.S., and C.Ø. conducted the experiments. S.S., S.F.G., I.D.Z., S.K., R.R.S., M.W.L., and C.S.E. analyzed data. C.S.E. wrote the manuscript. S.S., Y.P.-J, A.H.F., M.W.L., O.N.J., and C.S.E. supervised the project.

DECLARATION OF INTERESTS

S.S. and N.A. are, and M.W.L. and C.Ø. were, at the time of the making of this work, full-time employees of Roche Innovation Center Copenhagen. The remaining authors declare no competing interests.

REFERENCES

1. Merrill, A.H., Jr. (2011). Sphingolipid and glycosphingolipid metabolic pathways in the era of sphingolipidomics. Chem. Rev. *111*, 6387–6422.

2. Gomez-Muñoz, A., Presa, N., Gomez-Larrauri, A., Rivera, I.G., Trueba, M., and Ordoñez, M. (2016). Control of inflammatory responses by ceramide, sphingosine 1-phosphate and ceramide 1-phosphate. Prog. Lipid Res. *61*, 51–62.

3. Turpin-Nolan, S.M., and Brüning, J.C. (2020). The role of ceramides in metabolic disorders: When size and localization matters. Nat. Rev. Endocrinol. *16*, 224–233.

4. Tarasov, K., Ekroos, K., Suoniemi, M., Kauhanen, D., Sylvänne, T., Hurme, R., Gouni-Berthold, I., Berthold, H.K., Kleber, M.E., Laaksonen, R., and März, W. (2014). Molecular lipids identify cardiovascular risk and are efficiently lowered by simvastatin and *PCSK9* deficiency. J. Clin. Endocrinol. Metab. *99*, E45–E52.
5. Laaksonen, R., Ekroos, K., Sysi-Aho, M., Hilvo, M., Vihervaara, T., Kauhanen, D., Suoniemi, M., Hurme, R., März, W., Scharnagl, H., et al. (2016). Plasma ceramides predict cardiovascular death in patients with stable coronary artery disease and acute coronary syndromes beyond LDL-cholesterol. Eur. Heart J. *37*, 1967–1976.
6. Hilvo, M., Vasile, V.C., Donato, L.J., Hurme, R., and Laaksonen, R. (2020). Ceramides and ceramide scores: Clinical applications for cardiometabolic risk stratification. Front. Endocrinol. (Lausanne) *11*, 570628.
7. Neeland, I.J., Singh, S., McGuire, D.K., Vega, G.L., Roddy, T., Reilly, D.F., Castro-Perez, J., Kozlitina, J., and Scherer, P.E. (2018). Relation of plasma ceramides to visceral adiposity, insulin resistance and the development of type 2 diabetes mellitus: the Dallas Heart Study. Diabetologia *61*, 2570–2579.
8. Lemaitre, R.N., Yu, C., Hoofnagle, A., Hari, N., Jensen, P.N., Fretts, A.M., Umans, J.G., Howard, B.V., Sitlani, C.M., Siscovick, D.S., et al. (2018). Circulating sphingolipids, insulin, HOMA-IR, and HOMA-B: The Strong Heart Family Study. Diabetes *67*, 1663–1672.
9. Hilvo, M., Salonurmi, T., Havulinna, A.S., Kauhanen, D., Pedersen, E.R., Tell, G.S., Meyer, K., Teeriniemi, A.M., Laatikainen, T., Jousilahti, P., et al. (2018). Ceramide stearic to palmitic acid ratio predicts incident diabetes. Diabetologia *61*, 1424–1434.
10. Summers, S.A. (2018). Could ceramides become the new cholesterol? Cell Metab. *27*, 276–280.
11. Futerman, A.H., and Hannun, Y.A. (2004). The complex life of simple sphingolipids. EMBO Rep. *5*, 777–782.
12. Wegner, M.S., Schiffmann, S., Parnham, M.J., Geisslinger, G., and Grösch, S. (2016). The enigma of ceramide synthase regulation in mammalian cells. Prog. Lipid Res. *63*, 93–119.
13. Mullen, T.D., Hannun, Y.A., and Obeid, L.M. (2012). Ceramide synthases at the centre of sphingolipid metabolism and biology. Biochem. J. *441*, 789–802.
14. Park, J.W., Park, W.J., and Futerman, A.H. (2014). Ceramide synthases as potential targets for therapeutic intervention in human diseases. Biochim. Biophys. Acta *1841*, 671–681.
15. Tidhar, R., Zelnik, I.D., Volpert, G., Ben-Dor, S., Kelly, S., Merrill, A.H., Jr., and Futerman, A.H. (2018). Eleven residues determine the acyl chain specificity of ceramide synthases. J. Biol. Chem. *293*, 9912–9921.
16. Turpin-Nolan, S.M., Hammerschmidt, P., Chen, W., Jais, A., Timper, K., Awazawa, M., Brodesser, S., and Brüning, J.C. (2019). CerS1-derived $C_{18:0}$ ceramide in skeletal muscle promotes obesity-induced insulin resistance. Cell Rep. *26*, 1–10.e7.
17. Kremser, C., Klemm, A.L., van Uelft, M., Imgrund, S., Ginkel, C., Hartmann, D., and Willecke, K. (2013). Cell-type-specific expression pattern of ceramide synthase 2 protein in mouse tissues. Histochem. Cell Biol. *140*, 533–547.
18. Imgrund, S., Hartmann, D., Farwanah, H., Eckhardt, M., Sandhoff, R., Degen, J., Gieselmann, V., Sandhoff, K., and Willecke, K. (2009). Adult ceramide synthase 2 (CERS2)-deficient mice exhibit myelin sheath defects, cerebellar degeneration, and hepatocarcinomas. J. Biol. Chem. *284*, 33549–33560.
19. Pewzner-Jung, Y., Park, H., Laviad, E.L., Silva, L.C., Lahiri, S., Stiban, J., Erez-Roman, R., Brügger, B., Sachsenheimer, T., Wieland, F., et al. (2010). A critical role for ceramide synthase 2 in liver homeostasis: I. Alterations in lipid metabolic pathways. J. Biol. Chem. *285*, 10902–10910.
20. Pewzner-Jung, Y., Brenner, O., Braun, S., Laviad, E.L., Ben-Dor, S., Feldmesser, E., Horn-Saban, S., Amann-Zalcenstein, D., Raanan, C., Berkutzki, T., et al. (2010). A critical role for ceramide synthase 2 in liver homeostasis: II. Insights into molecular changes leading to hepatopathy. J. Biol. Chem. *285*, 10911–10923.
21. Park, J.W., Park, W.J., Kuperman, Y., Boura-Halfon, S., Pewzner-Jung, Y., and Futerman, A.H. (2013). Ablation of very long acyl chain sphingolipids causes hepatic insulin resistance in mice due to altered detergent-resistant membranes. Hepatology *57*, 525–532.
22. Gorski, M., van der Most, P.J., Teumer, A., Chu, A.Y., Li, M., Mijatovic, V., Nolte, I.M., Cocca, M., Taliun, D., Gomez, F., et al. (2017). 1000 Genomes-based meta-analysis identifies 10 novel loci for kidney function. Sci. Rep. *7*, 45040.
23. Wheeler, E., Leong, A., Liu, C.T., Hivert, M.F., Strawbridge, R.J., Podmore, C., Li, M., Yao, J., Sim, X., Hong, J., et al.; EPIC-CVD Consortium; EPIC-InterAct Consortium; Lifelines Cohort Study (2017). Impact of common genetic determinants of Hemoglobin A1c on type 2 diabetes risk and diagnosis in ancestrally diverse populations: A transethnic genome-wide meta-analysis. PLoS Med. *14*, e1002383.
24. Graham, S.E., Nielsen, J.B., Zawistowski, M., Zhou, W., Fritsche, L.G., Gabrielsen, M.E., Skogholt, A.H., Surakka, I., Hornsby, W.E., Fermin, D., et al. (2019). Sex-specific and pleiotropic effects underlying kidney function identified from GWAS meta-analysis. Nat. Commun. *10*, 1847.
25. Morris, A.P., Le, T.H., Wu, H., Akbarov, A., van der Most, P.J., Hemani, G., Smith, G.D., Mahajan, A., Gaulton, K.J., Nadkarni, G.N., et al. (2019). Trans-ethnic kidney function association study reveals putative causal genes and effects on kidney-specific disease aetiologies. Nat. Commun. *10*, 29.
26. Wuttke, M., Li, Y., Li, M., Sieber, K.B., Feitosa, M.F., Gorski, M., Tin, A., Wang, L., Chu, A.Y., Hoppmann, A., et al.; Lifelines Cohort Study; V.A. Million Veteran Program (2019). A catalog of genetic loci associated with kidney function from analyses of a million individuals. Nat. Genet. *51*, 957–972.
27. Turpin, S.M., Nicholls, H.T., Willmes, D.M., Mourier, A., Brodesser, S., Wunderlich, C.M., Mauer, J., Xu, E., Hammerschmidt, P., Brönneke, H.S., et al. (2014). Obesity-induced CerS6-dependent C16:0 ceramide production promotes weight gain and glucose intolerance. Cell Metab. *20*, 678–686.
28. Gosejacob, D., Jäger, P.S., Vom Dorp, K., Frejno, M., Carstensen, A.C., Köhnke, M., Degen, J., Dörmann, P., and Hoch, M. (2016). Ceramide synthase 5 is essential to maintain C16:0-ceramide pools and contributes to the development of diet-induced obesity. J. Biol. Chem. *291*, 6989–7003.
29. Hammerschmidt, P., Ostkotte, D., Nolte, H., Gerl, M.J., Jais, A., Brunner, H.L., Sprenger, H.G., Awazawa, M., Nicholls, H.T., Turpin-Nolan, S.M., Langer, T., et al. (2019). CerS6-derived sphingolipids interact with Mff and promote mitochondrial fragmentation in obesity. Cell *177*, 1536–1552.e3.
30. Raichur, S. (2020). Ceramide synthases are attractive drug targets for treating metabolic diseases. Front. Endocrinol. (Lausanne) *11*, 483.
31. Levin, A.A. (2019). Treating disease at the RNA level with oligonucleotides. N. Engl. J. Med. *380*, 57–70.
32. Straarup, E.M., Fisker, N., Hedtjärn, M., Lindholm, M.W., Rosenbohm, C., Aarup, V., Hansen, H.F., Ørum, H., Hansen, J.B., and Koch, T. (2010). Short locked nucleic acid antisense oligonucleotides potently reduce apolipoprotein B mRNA and serum cholesterol in mice and non-human primates. Nucleic Acids Res. *38*, 7100–7111.
33. Yu, R.Z., Graham, M.J., Post, N., Riney, S., Zanardi, T., Hall, S., Burkey, J., Shemesh, C.S., Prakash, T.P., Seth, P.P., et al. (2016). Disposition and pharmacology of a GalNAc3-conjugated ASO targeting human lipoprotein (a) in mice. Mol. Ther. Nucleic Acids *5*, e317.
34. Lindholm, M.W., Elmén, J., Fisker, N., Hansen, H.F., Persson, R., Møller, M.R., Rosenbohm, C., Ørum, H., Straarup, E.M., and Koch, T. (2012). PCSK9 LNA antisense oligonucleotides induce sustained reduction of LDL cholesterol in nonhuman primates. Mol. Ther. *20*, 376–381.
35. Butler, M., McKay, R.A., Popoff, I.J., Gaarde, W.A., Witchell, D., Murray, S.F., Dean, N.M., Bhanot, S., and Monia, B.P. (2002). Specific inhibition of PTEN expression reverses hyperglycemia in diabetic mice. Diabetes *51*, 1028–1034.
36. Wu, S., and Näär, A.M. (2019). SREBP1-dependent de novo fatty acid synthesis gene expression is elevated in malignant melanoma and represents a cellular survival trait. Sci. Rep. *9*, 10369.
37. Pendergraff, H., Schmidt, S., Vikeså, J., Weile, C., Øverup, C., W Lindholm, M., and Koch, T. (2020). Nuclear and cytoplasmatic quantification of unconjugated, label-free locked nucleic acid oligonucleotides. Nucleic Acid Ther. *30*, 4–13.
38. Prakash, T.P., Graham, M.J., Yu, J., Carty, R., Low, A., Chappell, A., Schmidt, K., Zhao, C., Aghajan, M., Murray, H.F., et al. (2014). Targeted delivery of antisense oligonucleotides to hepatocytes using triantennary *N*-acetyl galactosamine improves potency 10-fold in mice. Nucleic Acids Res. *42*, 8796–8807.
39. Javanbakht, H., Mueller, H., Walther, J., Zhou, X., Lopez, A., Pattupara, T., Blaising, J., Pedersen, L., Albæk, N., Jackerott, M., et al. (2018). Liver-targeted anti-HBV single-stranded oligonucleotides with locked nucleic acid potently reduce HBV gene expression in vivo. Mol. Ther. Nucleic Acids *11*, 441–454.

40. Weingärtner, A., Bethge, L., Weiss, L., Sternberger, M., and Lindholm, M.W. (2020). Less is more: Novel hepatocyte-targeted siRNA conjugates for treatment of liver-related disorders. Mol. Ther. Nucleic Acids *21*, 242–250.

41. van Poelgeest, E.P., Hodges, M.R., Moerland, M., Tessier, Y., Levin, A.A., Persson, R., Lindholm, M.W., Dumong Erichsen, K., Ørum, H., Cohen, A.F., and Burggraaf, J. (2015). Antisense-mediated reduction of proprotein convertase subtilisin/kexin type 9 (PCSK9): A first-in-human randomized, placebo-controlled trial. Br. J. Clin. Pharmacol. *80*, 1350–1361.

42. Moisan, A., Gubler, M., Zhang, J.D., Tessier, Y., Dumong Erichsen, K., Sewing, S., Gérard, R., Avignon, B., Huber, S., Benmansour, F., et al. (2017). Inhibition of EGF uptake by nephrotoxic antisense drugs in vitro and implications for preclinical safety profiling. Mol. Ther. Nucleic Acids *6*, 89–105.

43. Raichur, S., Brunner, B., Bielohuby, M., Hansen, G., Pfenninger, A., Wang, B., Bruning, J.C., Larsen, P.J., and Tennagels, N. (2019). The role of C16:0 ceramide in the development of obesity and type 2 diabetes: CerS6 inhibition as a novel therapeutic approach. Mol. Metab. *21*, 36–50.

44. Stein, C.A., Hansen, J.B., Lai, J., Wu, S., Voskresenskiy, A., Høg, A., Worm, J., Hedtjärn, M., Souleimanian, N., Miller, P., et al. (2010). Efficient gene silencing by delivery of locked nucleic acid antisense oligonucleotides, unassisted by transfection reagents. Nucleic Acids Res. *38*, e3.

45. Almeida, R., Pauling, J.K., Sokol, E., Hannibal-Bach, H.K., and Ejsing, C.S. (2015). Comprehensive lipidome analysis by shotgun lipidomics on a hybrid quadrupole-orbitrap-linear ion trap mass spectrometer. J. Am. Soc. Mass Spectrom. *26*, 133–148.

46. Sprenger, R.R., Hermansson, M., Neess, D., Becciolini, L.S., Sørensen, S.B., Fagerberg, R., Ecker, J., Liebisch, G., Jensen, O.N., Vance, D.E., et al. (2021). Lipid molecular timeline profiling reveals diurnal crosstalk between the liver and circulation. Cell Rep. *34*, 108710.

47. Laviad, E.L., Kelly, S., Merrill, A.H., Jr., and Futerman, A.H. (2012). Modulation of ceramide synthase activity via dimerization. J. Biol. Chem. *287*, 21025–21033.

48. Muir, A., Ramachandran, S., Roelants, F.M., Timmons, G., and Thorner, J. (2014). TORC2-dependent protein kinase Ypk1 phosphorylates ceramide synthase to stimulate synthesis of complex sphingolipids. eLife *3*, e03779.

49. Sassa, T., Hirayama, T., and Kihara, A. (2016). Enzyme activities of the ceramide synthases CERS2-6 are regulated by phosphorylation in the C-terminal region. J. Biol. Chem. *291*, 7477–7487.

50. Rajeev, K.G., Nair, J.K., Jayaraman, M., Charisse, K., Taneja, N., O'Shea, J., Willoughby, J.L., Yucius, K., Nguyen, T., Shulga-Morskaya, S., et al. (2015). Hepatocyte-specific delivery of siRNAs conjugated to novel non-nucleosidic trivalent *N*-acetylgalactosamine elicits robust gene silencing in vivo. ChemBioChem *16*, 903–908.

51. Freyre, C.A.C., Rauher, P.C., Ejsing, C.S., and Klemm, R.W. (2019). MIGA2 links mitochondria, the ER, and lipid droplets and promotes de novo lipogenesis in adipocytes. Mol. Cell *76*, 811–825.e14.

52. Sewing, S., Boess, F., Moisan, A., Bertinetti-Lapatki, C., Minz, T., Hedtjaern, M., Tessier, Y., Schuler, F., Singer, T., and Roth, A.B. (2016). Establishment of a predictive in vitro assay for assessment of the hepatotoxic potential of oligonucleotide drugs. PLoS ONE *11*, e0159431.

53. Tidhar, R., Ben-Dor, S., Wang, E., Kelly, S., Merrill, A.H., Jr., and Futerman, A.H. (2012). Acyl chain specificity of ceramide synthases is determined within a region of 150 residues in the Tram-Lag-CLN8 (TLC) domain. J. Biol. Chem. *287*, 3197–3206.

54. Lahiri, S., Lee, H., Mesicek, J., Fuks, Z., Haimovitz-Friedman, A., Kolesnick, R.N., and Futerman, A.H. (2007). Kinetic characterization of mammalian ceramide synthases: Determination of K_m values towards sphinganine. FEBS Lett. *581*, 5289–5294.

55. Ejsing, C.S., Sampaio, J.L., Surendranath, V., Duchoslav, E., Ekroos, K., Klemm, R.W., Simons, K., and Shevchenko, A. (2009). Global analysis of the yeast lipidome by quantitative shotgun mass spectrometry. Proc. Natl. Acad. Sci. USA *106*, 2136–2141.

56. Sampaio, J.L., Gerl, M.J., Klose, C., Ejsing, C.S., Beug, H., Simons, K., and Shevchenko, A. (2011). Membrane lipidome of an epithelial cell line. Proc. Natl. Acad. Sci. USA *108*, 1903–1907.

57. Fahy, E., Subramaniam, S., Murphy, R.C., Nishijima, M., Raetz, C.R., Shimizu, T., Spener, F., van Meer, G., Wakelam, M.J., and Dennis, E.A. (2009). Update of the LIPID MAPS comprehensive classification system for lipids. J. Lipid Res. *50* (*Suppl*), S9–S14.

58. Liebisch, G., Vizcaíno, J.A., Köfeler, H., Trötzmüller, M., Griffiths, W.J., Schmitz, G., Spener, F., and Wakelam, M.J.O. (2013). Shorthand notation for lipid structures derived from mass spectrometry. J. Lipid Res. *54*, 1523–1530.

59. Pauling, J.K., Hermansson, M., Hartler, J., Christiansen, K., Gallego, S.F., Peng, B., Ahrends, R., and Ejsing, C.S. (2017). Proposal for a common nomenclature for fragment ions in mass spectra of lipids. PLoS ONE *12*, e0188394.

60. Husen, P., Tarasov, K., Katafiasz, M., Sokol, E., Vogt, J., Baumgart, J., Nitsch, R., Ekroos, K., and Ejsing, C.S. (2013). Analysis of lipid experiments (ALEX): A software framework for analysis of high-resolution shotgun lipidomics data. PLoS ONE *8*, e79736.

61. Ellis, S.R., Paine, M.R.L., Eijkel, G.B., Pauling, J.K., Husen, P., Jervelund, M.W., Hermansson, M., Ejsing, C.S., and Heeren, R.M.A. (2018). Automated, parallel mass spectrometry imaging and structural identification of lipids. Nat. Methods *15*, 515–518.

62. Kovalchuk, S.I., Jensen, O.N., and Rogowska-Wrzesinska, A. (2019). FlashPack: Fast and simple preparation of ultrahigh-performance capillary columns for LC-MS. Mol. Cell. Proteomics *18*, 383–390.

63. Tyanova, S., Temu, T., and Cox, J. (2016). The MaxQuant computational platform for mass spectrometry-based shotgun proteomics. Nat. Protoc. *11*, 2301–2319.

64. Smyth, G.K. (2004). Linear models and empirical bayes methods for assessing differential expression in microarray experiments. Stat. Appl. Genet. Mol. Biol. *3*, Article3.